Intensity correlations in cavity QED

G. T. Foster, S. L. Mielke, and L. A. Orozco
Department of Physics and Astronomy, State University of New York, Stony Brook, New York 11794-3800
(Received 24 November 1999; published 18 April 2000)

The second-order intensity correlation function of light transmitted out of a cavity QED system exhibits the nonclassical features and dynamics of the atom-field interaction. We present measurements of the intensity correlation to examine the size of the nonclassical features and the dependence on driving intensity, detuning, and the strength of the atom-field coupling. We use a model that takes into account experimental conditions to achieve a quantitative agreement with the observations.

PACS number(s): 42.50.Dv, 42.50.Ct, 32.80.−t

I. INTRODUCTION

The second-order intensity correlation function is a sensitive probe of the quantum nature of light. Since quantum phenomena are intimately related to discrete changes, they manifest themselves on the intensity fluctuations of light. The correlation function quantifies the intensity fluctuations of light, and probes the system by performing a conditional measurement of the intensity in the time domain, with the possibility to reveal the underlying dynamics of the system. Nonclassical light fields exhibit intensity correlations which cannot be produced by a classical stochastic process.

A cavity QED system consisting of one or more two-level atoms coupled to a single mode of the electromagnetic field of an optical resonator has been important in elucidating the interaction of light with matter. Together with the laser and the optical parametric oscillator, cavity QED serves as a primary experimental system in quantum optics. The atom-cavity system, originally studied by Jaynes and Cummings [1], has evolved from optical bistability (OB) [2] to cavity QED. The evolution has not been serial; rather, the two areas developed, and many of the discoveries in OB are now part of cavity QED (see, for example, the contribution by Kimble in Ref. [3]).

Our work is preceeded by a long and distinguished list of explorations of the effects of strong coupling between an atom and a cavity, including vacuum Rabi splitting for an atom in an optical cavity [4,5], the micromaser [6], the microlaser [7], and the temporal evolution of both a microwave field probed by the state of a Rydberg atom [8] and the analog system of an ion in a rf trap [9]. Of fundamental importance to this paper is the observation and measurement of the second-order intensity correlation by Rempe *et al.* [10] that showed the nonclassical effect of antibunching in cavity QED. This work found that, unlike in resonance fluorescence, antibunching in cavity QED did not depend strongly on the number of atoms involved. Our measurements demonstrated a violation of the classical limitations placed on the delayed correlations, and also verified the intensity dependence of the oscillation frequency [11]. These initial findings merely scratched the surface. In particular, a significant difference existed between the measured correlations and the theoretical predictions. In this paper we present observations of the intensity correlation function, and show a quantitative agreement with a model incorporating experiment conditions. In addition, we show the dependence of the correlations on intracavity intensity, atomic detuning, and the number of atoms, along with qualitatively different intensity correlations with very large size.

The paper is organized as follows. In Sec. II, we describe theoretical models for the system. Section III discusses general characteristics of the intensity correlation function. Section IV reviews theoretical models, and discusses our modifications. Section V describes the apparatus and experimental procedures. We present our results in Sec. VI, and our conclusions in Sec. VII.

II. DESCRIPTION OF THE SYSTEM

The cavity QED system consists of a single mode of the electromagnetic field interacting with a collection of two-level atoms. The single mode of the field is defined by two spherical mirrors that form a standing-wave optical cavity. An optically pumped atomic beam crosses the mode waist. Dissipation plays an important role as both the atoms and the field couple to reservoirs. An atom can spontaneously emit light into cavity modes other than the preferred mode, and light inside the cavity can escape through the mirrors. The fractional solid angle subtended by the cavity mode is small enough ($\sim 10^{-3}$) that we do not have to make corrections to the atomic decay rates. We drive the system with a field injected through one of the mirrors. We detect the light that escapes from the cavity through the output mirror.

The work on OB [2] produced a large experimental and theoretical literature on the transmission properties of an optical cavity filled with two-level atoms. We use that knowledge to understand the structural features of the cavity QED system. These include effects that can be explained without considering quantum correlations between the atoms and the field, such as the transmission spectrum, characterized at low intensity by the vacuum Rabi doublet [12,13], and the time response to step excitation [14,15].

Several coupling rates characterize the interactions in the system. The coherent dipole coupling g_0 is defined as

$$g_0 = \left(\frac{\mu^2 \omega}{2\hbar \epsilon_0 V} \right)^{1/2}, \tag{1}$$

where μ is the transition dipole moment, ω is the transition frequency, and V is the cavity mode volume. There are three

dissipative rates; one for decay of the field from the cavity κ and one for decay of the atomic inversion $\gamma_\parallel = 1/\tau$ (τ is the radiative lifetime of the atomic transition) and polarization $\gamma_\perp$. For purely radiative decay, $\gamma_\parallel = 2\gamma_\perp$.

From the rates, we can construct two dimensionless numbers from the OB literature that are useful for characterizing cavity QED systems: the saturation photon number n_0 and the single atom cooperativity C_1. They scale the influence of a photon and the influence of an atom in the system. These two numbers relate the reversible dipole coupling between a single atom and the cavity mode (g_0) with the irreversible coupling to the reservoirs through cavity (κ) and atomic polarization and inversion decays ($\gamma_\perp, \gamma_\parallel$) by $C_1 = g_0^2/2\kappa\gamma_\perp$ and $n_0 = 2\gamma_\perp\gamma_\parallel/3g_0^2$. These two dimensionless numbers define the different regimes of OB and cavity QED. The strong-coupling regime of cavity QED $n_0 < 1$ and $C_1 > 1$ implies very large effects from the presence of a single photon and of a single atom in the system.

Three optical frequencies interact in the system: laser ω_l, cavity resonance ω_c, and atomic transition frequency ω_a. The driving laser field can be on or off resonance with the atomic transition or cavity resonance frequency, and so we define two normalized detunings: a cavity detuning $\Theta = (\omega_c - \omega_l)/\kappa$ and an atomic detuning $\Delta = (\omega_a - \omega_l)/\gamma_\perp$.

A. Quantum-mechanical model

The theoretical foundation for the interaction of a two-level atom and the quantized electromagnetic field was laid by Jaynes and Cummings [1].

The Hamiltonian for an isolated atom plus single field mode is

$$\hat{H} = \hbar\omega_a\hat{\sigma}^z + \hbar\omega_c\hat{a}^\dagger\hat{a} + \hbar g(\hat{\sigma}^+\hat{a} + \hat{a}^\dagger\hat{\sigma}^-), \tag{2}$$

where $\hat{\sigma}^\pm$ and $\hat{\sigma}^z$ are the the Pauli operators for raising, lowering, and inverting the atom, and $\hat{a}^\dagger$ and $\hat{a}$ are the raising and lowering operators for the field. The eigenvalues for Eq. (2) reveal the entanglement of the atom and field. The resulting coupled spectrum reveals a first excited state doublet, the vacuum Rabi doublet, with states shifted by $\pm g$ from the uncoupled resonance.

For our experimental system, a more precise description must consider N atoms and include interactions with the external environment, allowing the injection and escape of energy via a driving field, and dissipation into reservoirs. A master equation for the temporal evolution of the density matrix operator $\hat{\rho}$ can be derived using standard techniques (see, for example, Ref. [16]):

$$\begin{aligned}\dot{\hat{\rho}} = {} & \mathcal{E}[\hat{a}^\dagger - \hat{a}, \hat{\rho}] + g[\hat{a}^\dagger\hat{S}_- - \hat{a}\hat{S}_+, \hat{\rho}] \\ & + \kappa(2\hat{a}\hat{\rho}\hat{a}^\dagger - \hat{a}^\dagger\hat{a}\hat{\rho} - \hat{\rho}\hat{a}^\dagger\hat{a}) \\ & + \gamma_\perp\sum_{j=1}^{N}(2\hat{\sigma}_-^j\hat{\rho}\hat{\sigma}_+^j - \hat{\sigma}_+^j\hat{\sigma}_-^j\hat{\rho} - \hat{\rho}\hat{\sigma}_+^j\hat{\sigma}_-^j),\end{aligned} \tag{3}$$

where $\hat{\sigma}_-^j$ and $\hat{\sigma}_+^j$ are the lowering and raising operators for the jth two-level atom, and $\hat{S}_\pm = \Sigma_j\sigma_\pm^j$ are the collective raising and lowering operators for the atoms. $\mathcal{E}$ is the amplitude of the driving field, and g, κ, and $\gamma_\perp$ are the atom-cavity coupling rate, the cavity decay rate, and the atomic polarization decay rate as defined above.

In theory, we can calculate everything we want to know about the system from the master equation, as the expectation values of operators or products of operators. In practice, Eq. (3) does not have a general solution, so various approximations are made to obtain results which correspond to certain experimental regimes. We will consider these regimes and how they apply to our experiment when we consider different calculations for the intensity correlation below.

B. Semiclassical model

If we assume the atoms and field are decorrelated, $\langle\hat{a}^\dagger\hat{S}_\pm\rangle = \langle\hat{a}^\dagger\rangle\langle\hat{S}_\pm\rangle$, then the time evolution of the expectation values for the fields $\hat{a}^\dagger$ and $\hat{a}$ and atomic operators $\hat{\sigma}^\pm$ and $\hat{\sigma}^z$ result in the Maxwell-Bloch equations [17]

$$\frac{dx}{dt} = -\kappa(x - y - 2CP), \tag{4}$$

$$\frac{dP}{dt} = \gamma_\perp(xD - P), \tag{5}$$

$$\frac{dD}{dt} = -\gamma_\parallel\left[\frac{1}{2}(xP^* + x^*P) + D + 1\right], \tag{6}$$

with x^* and P^* following the complex conjugate equations of Eqs. (4) and (5), respectively. $x \equiv \langle\hat{a}\rangle/\sqrt{n_0}$ is the intracavity field with atoms and $y \equiv \mathcal{E}/\kappa\sqrt{n_0}$ is the field without atoms, where $\mathcal{E}$ is the input field amplitude (in units of 1/s). P is the normalized atomic polarization, and D is the normalized population difference between the upper and lower atomic states, with $D = -1$ representing all atoms in the ground state. $C = C_1N$ is the cooperativity parameter of OB for N effective atoms [18]. By setting the time derivatives to zero we can find a steady-state equation for the system relating x and y. From Eq. (4), we see that $y = x - 2CP$. With atoms, the cavity field x consists of the sum of the driving field y and the collective atomic polarization $2CP = -2Cx/(1 + |x|^2)$. For intermediate intensities ($x \sim 1$) the polarization is nonlinear, and can produce bistability in the transmitted field depending on the value of the parameter C. The system is linear for low intensities ($x \ll 1$):

$$y = x(1 + 2C). \tag{7}$$

Detunings shift the phase of the intracavity field with respect to the driving field [2], modifying Eq. (7) to

$$y = x\{[1 + 2C/(1 + \Delta^2)] + i[\Theta - 2C\Delta/(1 + \Delta^2)]\}. \tag{8}$$

The experimental system uses a standing-wave Gaussian mode cavity which modifies Eq. (7), but for weak fields the results are the same. We define the normalized driving inten-

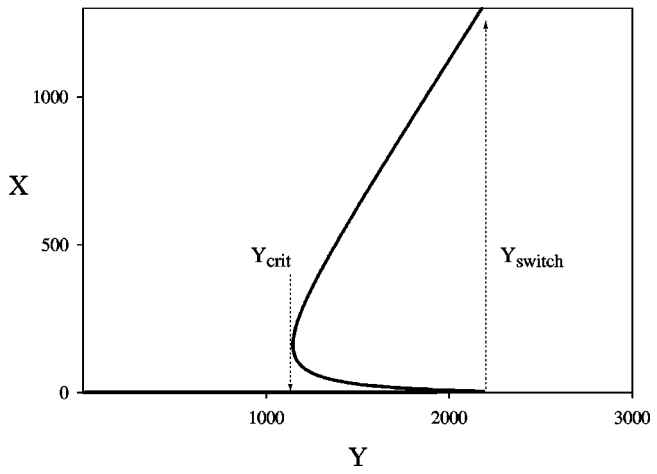

FIG. 1. Steady-state normalized transmited intensity (X) of a resonant OB system as a function of normalized driving intensity (Y) for C=37.5. Y_{crit} corresponds to the driving intensity at the entrance to the bistability region. Y_{switch} is the driving intensity at which the intracavity intensity switches to the upper branch.

sity $Y=y^2$ and the normalized intracavity intensity $X=|x|^2$. Figure 1 shows a plot of the intracavity intensity X versus the the driving intensity Y. The intracavity intensity exhibits bistability and hysteresis. As Y is increased into the nonlinear region past Y_{crit}, X remains on the lower branch until $Y=Y_{switch}$, at which point the intracavity intensity jumps to the upper branch value. Lowering Y, X remains at a high value until $Y<Y_{crit}$, at which point it jumps back down to the lower branch. We can define the values of X_{crit} and X_{switch}, which are the lower branch intracavity intensities corresponding to Y_{crit} and Y_{switch}, respectively.

III. CLASSICAL AND QUANTUM-MECHANICAL CORRELATION FUNCTIONS

We will briefly review the correlation function and its classical constraints. For a stationary process, the normalized second-order correlation function of the intensity is

$$g^{(2)}(\tau)=\frac{\langle I(t)I(t+\tau)\rangle}{\langle I(t)\rangle^2}, \tag{9}$$

where I is the average intensity. $g^{(2)}(\tau)$ is defined for an interval between t and $t+\tau$ and $g^{(2)}(\tau)=g^{(2)}(-\tau)$. At time $\tau=0$ we have $g^{(2)}(0)=\langle I^2\rangle/\langle I\rangle^2$. From this definition, $g^{(2)}(0)\geqslant 1$. For an ideal classical light source, such as a laser far above threshold, $g^{(2)}(0)=1$. A polarized thermal light source has $g^{(2)}(0)=2$. Fluctuations decorrelate at long times: $\tau\Rightarrow\infty$, $g^{(2)}(\tau)\Rightarrow 1$.

If the intensity $I(t)$ is a classical stochastic process, its two-time correlation function must obey the Schwarz inequality

$$|\langle z^*(t)z(t+\tau)\rangle|^2\leqslant\langle z^*(t)z(t)\rangle\langle z^*(t+\tau)z(t+\tau)\rangle. \tag{10}$$

From Eq. (10) there are two conditions on the correlation function $g^{(2)}(\tau)$ for classical fields [19]. The first is

$$g^{(2)}(0)\geqslant g^{(2)}(\tau). \tag{11}$$

$g^{(2)}(\tau)$ can never exceed its initial value. Violation of Eq. (11) is antibunching, where $g^{(2)}(0)<g^{(2)}(0^+)$ [20]. The second is more general:

$$|g^{(2)}(0)-1|\geqslant|g^{(2)}(\tau)-1|. \tag{12}$$

$g^{(2)}(\tau)$ can never be farther away from unity than it was at $\tau=0$. The violation of either of these implies a nonclassical electromagnetic field.

Quantum mechanically, the second-order correlation function of the intensity is [21]

$$g^{(2)}(\tau)=\frac{\langle\mathcal{T}{:}\hat{I}(t)\hat{I}(t+\tau){:}\rangle}{\langle\hat{I}(t)\rangle^2}, \tag{13}$$

where $\mathcal{T}$ denotes time ordering and the colons normal ordering. Here $\hat{I}(t)\equiv\hat{E}^\dagger(t)\hat{E}(t)$ is the intensity operator. To gain some insight into the relation of Eq. (13) to intensity fluctuations, we consider a single linearly polarized mode and positive frequencies, so that $\hat{E}\propto\hat{a}$. For a stationary process with $\tau=0$, we can rewrite Eq. (13):

$$g^{(2)}(0)=\frac{\langle\hat{a}^\dagger\hat{a}^\dagger\hat{a}\hat{a}\rangle}{\langle\hat{a}^\dagger\hat{a}\rangle^2}. \tag{14}$$

From the commutation relation $\hat{a}^\dagger\hat{a}=\hat{a}\hat{a}^\dagger-1$, and with $\hat{n}=\hat{a}^\dagger\hat{a}$ and a variance $\sigma^2=\langle\hat{n}^2\rangle-\langle\hat{n}\rangle^2$, we obtain

$$g^{(2)}(0)=1+\frac{\sigma^2-\langle\hat{n}\rangle}{\langle\hat{n}\rangle^2}. \tag{15}$$

The variance of the number of photons is related to probability of coincident photons given by $g^{(2)}(0)$. Light with Poissonian statistics has $g^{(2)}(0)=1$. Light with a super-Poissonian statistical distribution has $g^{(2)}(0)>1$. A sub-Poissonian distribution has $g^{(2)}(0)<1$, a clear signature of a nonclassical field. Light whose correlation function violates Eq. (11) could also be, but is not necessarily, sub-Poissonian.

From the quantum-mechanical definition of the correlation function in Eqs. (13) and (14), we see that it relies on the detection of a photon after a photon has already been detected. Using the quantum regression theorem, we can write the correlation function as [22]

$$g^{(2)}(\tau)=\frac{\langle\hat{I}(t)\rangle\langle\hat{I}(t+\tau)\rangle_c}{\langle\hat{I}\rangle^2}=\frac{\langle\hat{I}(\tau)\rangle_c}{\langle\hat{I}\rangle}, \tag{16}$$

where $\langle\hat{I}(\tau)\rangle_c$ is the mean light intensity at time τ conditioned on the event denoted by c.

Given a perfect series of photon arrival times, the correlation function $g^{(2)}(\tau)$ is calculated by assigning the first photon time $\tau=0$, and recording the arrival times of all successive photons with respect to the one at $\tau=0$. This process is then applied to the second photon, then the third, etc. A histogram is compiled of all the arrival times, and is normalized to the mean number of photons per unit time. The result

is a probability distribution for observing a photon at time τ, given that one was observed at time $\tau=0$, regardless of what happened in the intervening time. Equation (16) demonstrates this property by referring only to times t and τ. This is different than a waiting time distribution, in which a histogram is compiled of the time intervals between successive pairs of photons. The waiting time distribution gives information about the probability of observing a photon at time τ, given that one was detected at $\tau=0$, and that no photons were observed between the two times. For $\tau\rightarrow\infty$, the correlation function has a mean value of 1, while the waiting time distribution has a mean value of 0. For times much shorter than the average time between photoelectric counts, the waiting time distribution is proportional to $g^{(2)}(\tau)$ [23], a situation achievable in the limit of low intensity, or for low detector efficiency. It is important to note that the correlation function measurement is independent of detector efficiencies and any linear losses in the system (beam splitters, cavity) [21].

IV. CALCULATIONS OF THE CORRELATION FUNCTION IN CAVITY QED

There are several approaches in the literature for finding a theoretical expression for $g^{(2)}(\tau)$ for this system. Calculations were performed in the context of OB [2], but we consider approaches that are more directly applicable to a strongly coupled cavity QED system. The state of the system can be described by a density operator with its time evolution determined by a master equation. The first method, applied by Carmichael *et al.* [24], solves the master equation by assuming that the system has at most two excitations. The second method, followed by Carmichael [25] and later extended by Brecha *et al.* [22], relies on the assumption that $(n_0, N_1 \equiv 1/C_1) \gg 1$. Recently, a numerical approach using quantum Monte Carlo simulations provided new insight into the system [26,27].

We briefly summarize the two analytic theories. These serve as a basis for our theoretical comparison, which takes into account the effect of using an atomic beam.

A. Low-intensity theory for $g^{(2)}(\tau)$

Starting with Eq. (3), we expand the density-matrix operator $\hat{\rho}$ to lowest order in $\mathcal{E}/\kappa$, retaining states with zero, one, or two quanta of energy. By taking a weak-field limit, the result does not rely on assumptions about system size as characterized by $n_0, N, 1/C_1 \gg 1$. From the steady state, $g^{(2)}(\tau)$ can be calculated as the conditional intensity given that a photon was detected from the cavity. Carmichael *et al.* [24] calculated the resulting form for $g^{(2)}(\tau)$ for $\tau>0$,

$$g^{(2)}(\tau)=|1+\mathcal{A}\mathcal{F}(\tau)|^2, \tag{17}$$

where $\mathcal{F}$ is a decaying oscillation,

$$\mathcal{F}=e^{-\beta\tau}[\cos(\Omega_0\tau)+(\beta/\Omega_0)\sin(\Omega_0\tau)], \tag{18}$$

with $\beta\equiv(\kappa+\gamma_\perp)/2$ representing the average decay rate and Ω_0 the vacuum Rabi frequency in the low intensity limit:

$$\Omega_0=\sqrt{g^2N-\frac{(\kappa-\gamma_\perp)^2}{4}}. \tag{19}$$

The amplitude of the decaying oscillations is given by

$$\mathcal{A}=-\frac{4C_1^2N}{(1+\gamma_\perp/\kappa)(1+2C_1N)-2C_1}. \tag{20}$$

$\mathcal{A}$ is the ratio of the change in the field to the mean field given that a photon is emitted. On resonance and for strong coupling, this change will always be negative. As the coupling constant g increases, C_1 increases and so does the size of the discontinuity, which grows relative to the steady-state amplitude x. For very large coupling constants (large C_1), the jump can be many times larger than the intracavity field x. The effects in this system are largely independent of N since, for large N, $\mathcal{A}$ is proportional to C_1: $\mathcal{A}\approx-2C_1/(1+\gamma_\perp/\kappa)+O(1/N)$. The weak dependence of the size of the effect on the number of atoms is one distinguishing feature compared to resonance flurorescence, and was demonstrated in the initial antibunching measurements carried out by Rempe *et al.* [10].

The jump occurs because the polarization of the medium increases when a photon leaves the cavity. The collective cavity enhancement of the dipole decay rate is reduced in the ratio $(N-1)/N$, and this increases the polarization amplitude (which is inversely proportional to the damping rate). Interestingly, this is a different mechanism for production of nonclassical light than that of resonance fluorescence. In this case the antibunching with $g^{(2)}(0)=0$ results from the fact that when an atom emits a photon, it has to be reexcited before it can emit a second photon. In cavity QED, N atoms collectively form a polarization which can exactly cancel the driving field at some time $\tau\geqslant0$ following a photon emission. Depending on the parameters, the $\tau=0$ jump in the polarization can reverse the phase of the cavity field, and the resulting correlation function can exhibit bunching. Figure 2 shows the time evolution of the field and the resulting intensity correlation at $\tau>0$. Following the jump in the polarization, the system evolves back to a steady state with a decaying oscillatory response exhibiting the coherent coupling of the polarization field emitted from the atoms and the cavity field. The oscillations can also be viewed as an interference between the driving field and the forward scattered field from the atoms [22,24].

B. Small-noise expansion

Carmichael [25] and Brecha *et al.* [22] made use of small-noise approximations, i.e., $n_0\gg1$ and $N\gg1$, to solve for the $g^{(2)}(\tau)$. Using the positive-P representation, they converted Eq. (3) into a Fokker-Planck equation, and then into an equivalent set of Ito stochastic differential equations. The resulting drift matrix that detemines the time evolution of the system is the same as the Maxwell-Bloch equations. The main benefit of this approach is that homogeneous broadening can be included. This is characterized by the parameter Γ, where $\Gamma=\gamma_\parallel/2\gamma_\perp$.

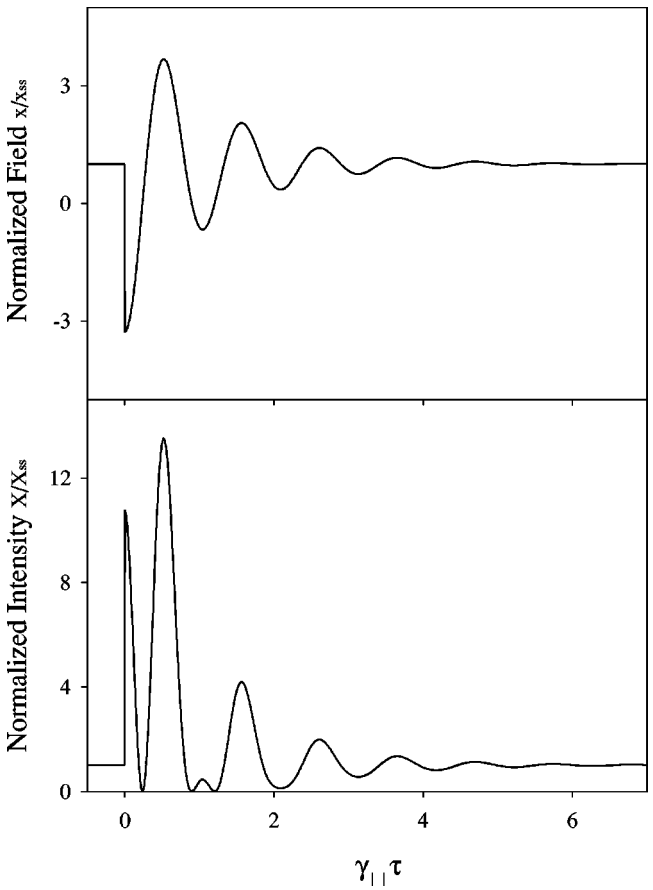

FIG. 2. The top plot shows the dynamical response of the field for $\tau>0$ conditioned on a photon detection at $\tau=0$. The size of the jump in the field is determined by the system parameters, and is given by $\mathcal{A}$. The field is normalized by the steady-state field (x_{ss}). The bottom plot shows the resulting normalized intensity. The change in phase of the field results in a peak at $\tau=0$. The parameters are $g=11.6$ MHz, $\kappa=7.9$ MHz, and $N=10$ atoms. The time axis is scaled in units of $\gamma_{\parallel}$.

C. Modifications to theory

Several experimental realities are not considered in the available theories. Full-scale quantum trajectory simulations including the atomic beam and mode structure are beginning to achieve quantitative agreement with our correlation measurements [26]. Most of the discrepancies can be traced to the atomic beam. A second significant effect is operating the system at a low enough intensity to justify use of the weak-field theories.

Significant effects arise from the use of a thermal atomic beam as the source of our atoms. These are transit broadening due to the finite interaction time of the atoms crossing the cavity mode, the random atomic spatial distribution crossing the standing-wave Gaussian mode, number fluctuations of the number of atoms interacting with the field, and inhomogeneous broadening of the transition from inperfect alignment and collimation of the atomic beam. We comment on these effects, and on how we model them for our system below.

1. Transit broadening

The atoms cross the Gaussian mode waist with a thermal velocity, with a typical most probable velocity $v_p\approx 350$ m/s. We model this as a homogeneous broadening process which increases the polarization decay rate. To estimate the transit effect, we reference previous calculations done for experiments studying OB [28], which allow us to determine the amount by which the $\gamma_{\perp}$ is scaled. Specifically, the authors of Ref. [28] calculated the effects of a thermal velocity distribution of atoms traversing a Gaussian mode on the absorption as a function of the normalized intracavity intensity, X. The parameters for our system fall into the range of transit times considered in Ref. [28]. We can then make use of the linearized theory for $g^{(2)}(\tau)$ of Brecha, with a $\Gamma<1$ to estimate the effect. We assume that the homogeneous broadening gives an overall scaling which we can determine by comparing the values of $g^{(2)}(0)$ for $\Gamma=1$ and the estimated reduced Γ for the particular cavity parameters. Transit time effects were also examined by Clemens and Rice [27].

2. Effective atoms

Atoms in the beam pass with a random distribution through the standing-wave Gaussian structure of the cavity mode. The number of atoms that we measure is an average of strongly and weakly coupled atoms. Based on numerical beam simulations, the actual total number of contributing atoms is a factor of ~ 10 larger [29]. In an effort to correct for the effects of atoms that are randomly distributed in the cavity, Rempe *et al.* [10] extended Eq. (17) by using a basis in which the atoms are considered individually. Each atom has an effective coupling based on its location in the mode. The result is nearly identical to Eq. (17), except that instead of $\mathcal{A}$ one has a summation which includes contributions from all the atoms distributed within the standing-wave Gaussian cavity mode.

3. Atom number fluctuations

Number fluctuations play an important role when we operate with a low mean effective number of atoms. Poissonian fluctuations of the number of atoms alter both the effective coupling frequency $g_0\sqrt{N}$ and the overall transmission of the cavity system through the cooperativity C and Eq. (7). These effects are most pronounced for low effective numbers of atoms. Our intensity correlation measurement is sensitive to beam fluctuations which will have a correlation time given by the mean transit time of the atoms. These intensity fluctuations are not taken into account by the models, in particular since all models assume a fixed number of atoms in a weak field. The observational consequence depends on the beam flux. At low beam intensities (≈ 1 atom), a large bunched peak can arise as the large fluctuations in the atom number cause random intensity fluctuations in the cavity transmission. At larger effective atom numbers, we can consider the effect of number fluctuations through changes in the frequency of oscillation. Averaging the expression for $g^{(2)}(\tau)$ [Eq. (17)] for a series of realizations with $N+\Delta N$, where ΔN is a random number from a normal distribution with $\sigma=\sqrt{N}$, will average out zeros in the correlation func-

tion at delayed times. Although the amplitude of the polarization does not depend strongly on N, the oscillation frequency scales like $\sqrt{N}$. To simulate the effect of number fluctuations, as well as the Gaussian standing wave mode, full quantum trajectory Monte Carlo simulations are required.

4. Inhomogeneous broadening

Doppler broadening can significantly reduce the observed correlations. If the beam crosses the cavity mode at an angle θ from perpendicular, the otherwise tightly collimated beam acquires a tranverse velocity component in the direction of the mode, $v_y = v_p \sin(\theta)$, which causes the light interacting with the atoms to acquire a Doppler shift $\vec{k} \cdot \vec{v}$. The velocity spread of the beam yields a spread in Doppler shifts and detunings Δ relative to the excitation laser frequency.

5. Outside of the weak-field limit

To obtain a good signal-to-noise ratio in a reasonable counting time, we operate the system in a regime where we may not be in the weak-field limit. In terms of the weak-field theory [Eq. (17)], there is an appreciable probability to have more than two excitations in the system. We have investigated the size of nonclassical effects as a function of the intracavity intensity.

6. Laser and cavity jitter

Laser and cavity jitter can be accounted for by considering an average over repeated realizations of $g^{(2)}(\tau)$ with the cavity detuning Θ or the atomic detuning Δ fluctuating either with Gaussian or evenly distributed fluctuations. These will tend to reduce the size of the correlations. In practice, the cavity lock and laser lock are stable enough to ignore these effects.

D. Experimental model

We use the weak-field theory given by Eq. (17) as the basis for our theoretical comparisons. Detunings can be included by replacing κ with $\kappa(1+i\Theta)$ and $\gamma_\parallel$ with $\gamma_\parallel(1+i\Delta)$ [22]. The tilt ϕ of the cavity mode from perpendicular to the atomic beam introduces Doppler shifts of the excitation laser frequency due to the tranverse velocity component of the atoms, $v \sin\phi$. We model this as an atomic detuning $\Delta = v \sin\phi/\lambda/\gamma_\perp$. The velocities of the atoms in the cavity follow a Maxwell-Boltzmann distribution [28]. We perform a weighted summation of the conditioned field $(\mathcal{A}\mathcal{F}(\tau))$ for a range of atomic detunings Δ with weight given by a Maxwell-Boltzmann distribution. The intensity correlation is then given by Eq. (17) using the weighted sum for $\mathcal{A}\mathcal{F}(\tau)$. We independently determine the mean atomic velocity from the oven temperature, and determine the tilt angle from the laser frequency shift that minimizes the transmission. This is the most important contribution to bring the theory and the experiment in agreement.

Atomic number fluctuations and the random distribution of atoms in the mode are taken into account as follows. For a given mean number of atoms, which can be determined from g, and the measured oscillation frequency $g\sqrt{N}$ observed in the correlations, we sum the conditional intensity for different numbers of atoms N_i with a weighting given by a Poissonian distribution with mean N. For each N_i in the sum, we perform the sum over the detuning distribution discussed above, and also do a set of averages of the different atom distributions that takes into account less than optimal coupling [10]. The averaging over repeated random distribution yields an effective $\mathcal{A}$ reduced to roughly one-half the value predicted by Eq. (17). Finally we include transit broadening effects as a homogeneous process that scales $\mathcal{A}\mathcal{F}$ based on the change in $g^{(2)}(0)$ determined from the small noise theory [22]. The experimental Γ is estimated from OB calculations [28].

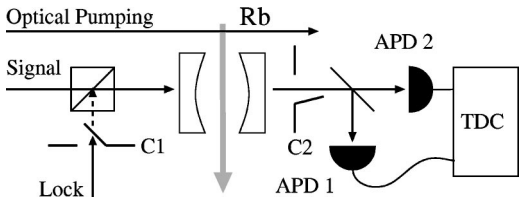

FIG. 3. Simplified diagram of the experimental setup. The Rb atomic beam is optically pumped before entering the cavity. The lock beam passes through a chopper wheel ($C1$) before being recombined with the input signal beam. We detect photons in the transmitted signal in an alternating cycle with the lock. The chopper ($C2$) blocks the transmitted signal path whenever the lock is open.

V. APPARATUS AND PROCEDURE

The experiment consists of four key components: the cavity, the atomic beam, an excitation laser, and the detector system. Figure 3 shows the general setup of the experiment. We drive the cavity system from one side, and observe the transmitted light out the other.

The heart of the experiment is the optical cavity. This is formed by two high-reflectivity curved mirrors coated by Research Electro-Optics. Table I shows the specific parameters for the cavities employed in these experiments. Each mirror is mounted to a stainless-steel holder which is inserted into a stainless-steel tube with a collimating slit. Piezoelectric transducers attached to the mirror holders allow us to control the mirror spacing. During measurements, a feedback loop holds the cavity on the TEM_{00} resonance. The cavity tube rests on a stack of sorbothane and lead, which provides

TABLE I. Cavity parameters: cavity waist w_0, mirror separation d, atom-cavity coupling $g/2\pi$, cavity decay rate κ, saturation photon number n_0, single-atom cooperativity C_1, slit width w, and cavity input and output mirror curvatures $r_1 r_2$.

Cavity	w_0 (μm)	d (μm)	$g/2\pi$ (MHz)	κ (MHz)	n_0	C_1	w (μm)	$r_1 r_2$ (cm)
1	29.7	507	7.75	1.75	0.2	5.7	200	5 5
2	26.6	325	10.8	2.6	0.11	7.4	50	5 5
3	33.6	83	16.9	4.85	0.04	9.7	50	50 50
4	21.5	430	11.6	7.9	0.09	2.8	50	1 5

isolation from mechanical vibrations.

A thermal beam of Rb atoms is produced from an effusive oven 35 cm from the cavity, in a chamber pumped by a large diffusion pump. Collimation comes from a water-cooled copper plate 5 cm from the oven opening, and a 3-mm slit 5 cm further downstream. Final collimation is provided by the 50–200-μm slit in the cavity holder. The oven is heated to $\approx$430 K. A computer-controlled feedback system maintains the temperature of the oven within ± 0.1 K. The 1-mm-wide oven opening and the aperture before the cavity form a beam with an angular spread of 3.4 mrad. A welded bellows provides vibration isolation between a diffusion pump and a six-way cross containing the cavity. Typical operating pressures are around 5×10^{-7} torr. A liquid-nitrogen-cooled Cu sleeve surrounds the cavity to reduce background atomic vapor. The presence of a background atomic vapor destroys the observed correlations.

The excitation source for the experiment is an Ar^{+}-pumped titanium sapphire (Ti:sapphire) laser, a modified Coherent 899-01. The laser beam is split into a signal beam and auxiliary beams for laser frequency locking, cavity locking, and optical pumping. We lock the frequency of the laser with the Pound Drever Hall technique [30]. An auxillary beam has 12-MHz sidebands put on it with an elecro-optic modulator (EOM). This beam is used as a probe for saturation spectroscopy in a Rb vapor cell and detected with a fast photodetector. The linewidth of the laser is less than 200 kHz over 1 s, as measured independently on a Fabry-Perot fringe with detection bandwidth of $\approx$400 kHz. The signal and lock beams are on resonance with the $5S_{1/2},F=3\rightarrow5P_{3/2},F=4$ transition of ^{85}Rb at 780 nm. A double-passed acoustic-optic modulator in the laser lock allows us to adjust its frequency around the Rb resonance.

An optical pumping beam of diameter 2 mm, parallel to the cavity mode, intersects the atomic beam 1 cm before the atoms enter the cavity. The atoms are excited into the strong cycling transition $5S_{1/2},F=3,m_F=3\rightarrow5P_{3/2},F=4,m_F=4$. A 2.5-G uniform magnetic field applied along the axis of the cavity provides a quantization axis such that the circular polarization of the optical pumping beam takes all the atoms into the ground-state magnetic sublevel $F=3,m_F=3$. When the oven is on, we look at the fluorescence perpendicular to the optical pumping beam—atomic beam plane. The fluorescence is imaged onto a photomultiplier. When we scan the laser frequency, we observe a fluorescence peak. We simultaneously compare the peak with an auxiliary saturation spectroscopy signal, and make adjustments to the optical pumping alignment to ensure that it is perpendicular to the atomic beam. We also adjust the pumping power to minimize any peak present from the $5S_{1/2},F=3\rightarrow5P_{3/2},F=3$ transition. We test the quality of the optical pumping by making measurements of the transmission of the cavity with and without optical pumping.

Another EOM generates fm sidebands on the lock beam. The reflected lock beam is used to hold the cavity on resonance. During data collection, we send the beam through a chopper wheel which alternately passes the lock beam and opens the path from the cavity to the photon counting detectors at $\approx$1.1 kHz. The lock beam is blocked for a longer time than the signal path is open, ensuring that no lock beam light enters the cavity while we collect data. The duty cycle of the open and/or closed signal is typically 1/3.

The lock and signal beams have orthogonal linear polarizations when they are combined at a nonpolarizing beam splitter before the cavity. The resulting beam is sent through a $\lambda/4$ plate and mode matched into the cavity with typically more than 90% of the signal beam intensity into the TEM_{00} mode. The circular polarization is in the same sense as the optical pumping beam. On the output side of the cavity, the beam passes through another $\lambda/4$ plate before a polarizing beam splitter sends the lock beam to a photomultiplier. The signal beam is directed to the photon correlator, passing through the chopper wheel on the way.

The photon correlator consists of two avalanche photodiodes (APD's) EG&G SPCM-AQ-151 behind an unpolarized 50-50 beam splitter. These detectors have a quantum efficiency of 50%, a less than 50-Hz dark count rate, and a dead time of 30 ns. The detector electronics produce a transistor-transistor logic pulse for each photon detection. An unfortunate property of APD's is the light emitted from the APD's during the avalanche process [31]. Since the detectors are mode matched to the cavity output, light emitted from the one APD can reflect from the cavity and enter the other APD, causing false counts. The emission is broadband and unpolarized, so a combination of spectral filters and polarizers in front of the APD's alleviates the problem. The spectral filters are an Andover 10-nm-wide interference filter with 88% peak transmission, and a piece of anti-reflection-coated Schott RG-9 glass, which significantly attenuates wavelengths greater than 1 μm. The total transmission at 780 nm is 84%.

Pulses from the start APD serve as the triggers for a Lecroy 3377 time to digital converter (TDC) which registers the arrival time of up to 16 pulses from the stop APD with 0.5-ns resolution. The TDC registers hits for a 1-μs count interval per start. The timing data are transfered across a CAMAC (computer automated measurement and control) crate to a Lecroy 4302 memory module that stores up to 16 000 hits. When the memory is full, the data are transfered over a general purpose interface bus to a computer. A program controls the collection, histogramming and plotting the data.

The pulses from the APD's pass through a series of gates, logic boxes, and delays before arriving at the TDC. The pulses from the start detector are gated, so that additional pulses from the start detector are blocked from retriggering the TDC. Both the start and stop pulses are then gated with a signal derived from the chopper wheel, so that pulses reach the TDC only when the signal is open and the lock beam blocked. We also can discriminate the cavity lock and logically AND this with the chopper gate to only allow counts when the cavity is on resonance. The stop pulses are delayed by $\approx$400 ns to allows us to see zero delay coicidences. A copy of the pulses from each detector goes to a Stanford Research Systems SR400 photon counter which measures the count rates from each APD. These rates yield the mean intensity of the light emitted from the cavity after correcting for efficiencies and linear losses. We have extensively tested

the performance of the photon correlator system in the past, studying the correlation functions of a noise-driven diode laser [32].

We independently measure the time delay between the start and stop paths using a 10 kHz pulser. This determines the bin corresponding to $\tau=0$. Typical minimum gated counting rates are 5 kHz, with a gated background rate of 500 Hz. Ideally we would operate at a lower counting rate, but the data collection time becomes prohibitively long. At the minimum counting rate, we collect data for approximately 30 min.

During a data collection run, we first let the oven temperature stabilize and lock its temperature using a simple proportional current on-off cycle feedback program. We can change the number of atoms in the cavity by varying the oven temperature in a controlled manner. After we verify the prescence of an atomic beam, we take a sample $g^{(2)}(\tau)$ measurement. This can give us an idea about whether we are close to resonance.

We use the oscillation frequency from a low-intensity correlation measurement to determine $g\sqrt{N}$. The frequency is independent of the cavity mode geometry at low intracavity fields. As a second check, we measure the ratio of transmitted intensity without atoms ($\propto Y$) to the intensity with atoms ($\propto X$), which gives C using Eq. (7).

We attempt to align the cavity mode as close as possible to perpendicular to the atomic beam path. Imperfect alignment and a shift in the cavity mode during cooling can lead to a tilt from perpendicular of as much as 1°. We adjust the laser frequency to compensate for the Doppler shift of the atomic response using our knowledge from OB equation (8): the transmission out of the cavity is minimized on resonance. While observing the cavity transmission with the APD's, we adjust the laser frequency to find the minima. A detuning $\Delta=1$ (3 MHz for Rb) increases the transmission by a factor of 2. In practice, we also use the correlation measurement itself to find the optimal detuning that minimizes $g^{(2)}(0)$.

We make use of the following relation to determine the intracavity intensity normalized by the saturation photon number [28] from the power P estimated at the cavity output:

$$X=\frac{3P}{\pi w_0^2 I_{sat} T}. \tag{21}$$

$I_{sat}=\pi\hbar\omega/(3\tau\lambda^2)$ (1.7 mW/cm^2 in Rb) is the saturation intensity of the atom with transition frequency ω and lifetime τ. T is the output mirror transmission. A simpler expression relates the output flux R to the intracavity photon number by the cavity decay rate κ: $n_0 X=R/(2\kappa)$. The overall uncertainty in the determination of X is $\approx 20\%$.

VI. RESULTS

We have systematically probed the intensity correlation function of the cavity QED system. This has revealed the damped oscillatory frequency response characteristic of this system and nonclassical features of the correlations, including sub-Poissonian statistics, antibunching, and new violations at delayed times of the Schwarz inequality. Our studies have also provided important evidence to point to the origin of the features as an inteference of the cavity field and the atomic polarization field. As a consequence of the strong coupling of the system, the interference can give rise to interesting correlation functions qualitatively different from that attainable in resonance fluorescence.

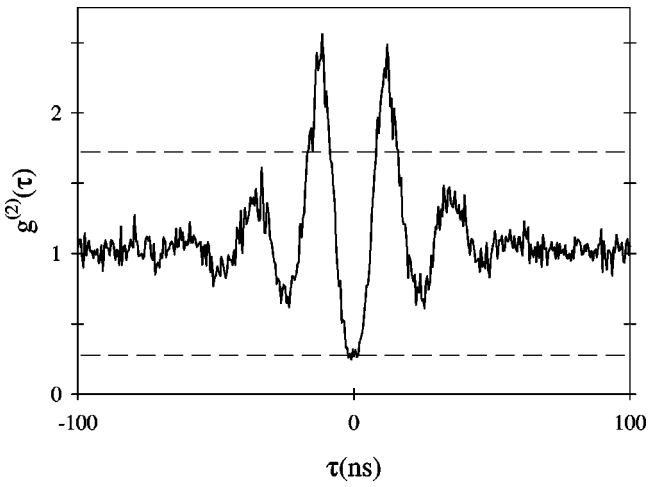

FIG. 4. Second-order intensity correlation for a strongly coupled cavity QED system. This is data collected with cavity 4 with $\bar{N}\approx 13$ atoms. The intracavity intensity $X=0.084$. The dashed lines show the limits placed by the Schwarz inequality on $g^{(2)}(\tau)$.

The results are organized as follows. First we review our findings about the general features of the correlation function, considering the kind of nonclassical violations and the dynamical behavior. We present measurements which demonstrate large sub-Poissonian statistics and how the nonclassical feature disappears as the intracavity intensity increases. A comparison is made between our low-intensity data and the theory. Next we present results of the effect of introducing a detuning between the excitation laser and the atoms. Then we show how the correlations change as the system coupling is increased. Finally we also present measurements as a function of the number of atoms.

A. General features of the correlation function

Figure 4 presents a typical correlation function that can be measured using cavity 4 (see Table I). The plot shows raw data normalized to the long-time mean counts. The long-time mean agrees with the observed levels within the uncertainty of our counting measurements. The data collection time was 2 min, with a mean of 200 counts per bin at long times. The correlation function is nonclassical, as it is antibunched [positive curvature at $\tau=0$, Eq. (11)] and exhibits sub-Poissonian statistics, with $g^{(2)}(0)=0.30\pm 0.02$. In addition, the delayed response at the first peaks at $\tau\approx\pm 10$ ns violates the second Schwarz condition [Eq. (12)]. Classically, we would expect a detector to click most often during fluctuations up in the intensity, and we should have a peak at $g^{(2)}(0)$.

The quantum-mechanical picture of the effect of an escape of a photon is that it causes the polarization field to jump. This is out of phase with the cavity field, and causes a decrease in this field. This explains why the conditional

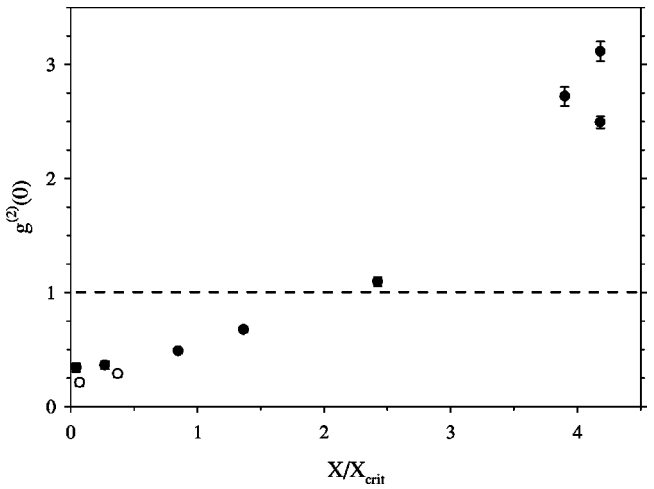

FIG. 5. Change in $g^{(2)}(0)$ as a function of normalized intracavity intensity X/X_{crit}. The data were taken with cavity 4 on resonance. The two unfilled data points at low intensity are from a separate data collection with the same cavity and number of atoms ($N \approx 13$).

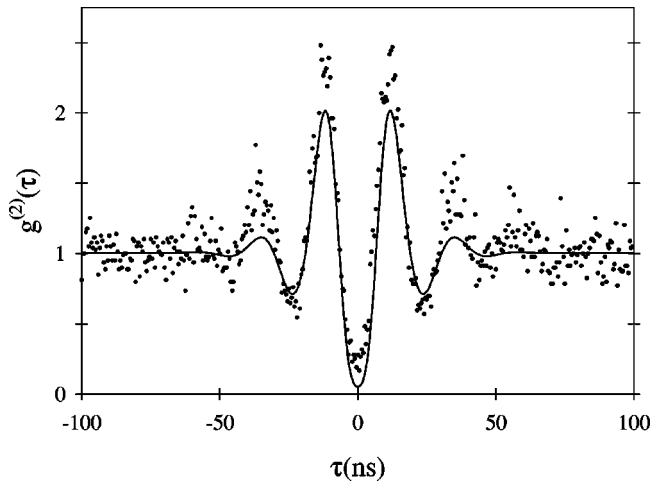

FIG. 6. Data taken with cavity 4 on resonance at weak excitation corresponding to the lowest intensity point in Fig. 5 with $X = 0.02$ (open circle). This corresponds to a mean intracavity photon number of $Xn_0 = 2 \times 10^{-3}$. The continuous line shows the results from the model.

probability to detect a second photon is reduced. In time, the system evolves back to a steady state between the atomic polarization and the driving field. This is characterized by a decaying oscillation at the Rabi frequency of the system, $g\sqrt{N}$. The decay is set by the average of the cavity and radiative atomic decay rates. In our experimental system the apparent decay is faster because transit and inhomogeneous broadenings increase the atomic decay rate ($\gamma_\perp$). These broadening mechanisms dephase the interference between the polarization and driving field, which significantly reduces the size of the nonclassical effects.

We have previously shown that the oscillation frequency of the system decreases as the driving intensity increases [11]. This is the opposite of what occurs in resonance fluorescence [21]. In a coupled atom-cavity system, the coupling between the atoms and cavity decreases with increasing input intensity [12,13], and so does the frequency of oscillation. The evolution of the oscillation frequency observed in the correlation functions can be determined by calculating the eigenvalues of the linearized Maxwell-Bloch equations by use of the quantum regression theorem [33]. This accurately describes the evolution when the Gaussian standing-wave nature of the cavity mode is included.

B. Intensity dependence

Theoretical descriptions for $g^{(2)}(\tau)$ assume a weak-field limit. We have probed the response of our system to low intracavity intensities. The saturation of nonclassical statistics is evident in Fig. 5. We have plotted $g^{(2)}(0)$ as a function of the normalized intracavity intensity X/X_{crit}. X_{crit} is the intracavity intensity at the entrance of the bistable intensity region (see Fig. 1). We obtain the largest nonclassical character as measured by $g^{(2)}(0)$ for low intensities. The sub-Poissonian nature disappears in the nonlinear bistability region. As the intensity is further increased, the cavity transmission becomes noisier and strongly bunched. This region is characterized by anharmonicity in the frequency spectrum [13]. This can act to amplify small fluctuations in the cavity detuning that can translate into large intensity fluctuations. The spread in $g^{(2)}(0)$ at high intensity reveals the unstable nature of the region near to the switching point, where the harmonic doublet is closer together. This switching point corresponds to $X/X_{crit} = 5.22$. Monte Carlo quantum trajectory simulations are required to simulate the behavior of the system with a high excitation. At low intensity, the two unfilled circles are measurements with the same cavity parameters, but taken during a separate data collection. The main difference was the tilt of the mode from perpendicular to the atomic beam as discussed above. The unfilled circles had an angle of 17.3 mrad, while the filled circles had a 12.2-mrad angle. There is also uncertainty in the value of X/X_{crit} between the two data collections due to differences in the alignment of the mode to the detector.

At low excitation, we can obtain quantitative agreement with the weak-field theory by including experimental effects. Figure 6 shows the correlation function with $g^{(2)}(0) = 0.20 \pm 0.02$. This is the largest nonclassical effect observed in our cavity QED system, corresponding to a fivefold reduction of the Poissonian noise compared to a laser field. Both classical conditions set by the Schwarz inequality are also violated. This is with $N = 13.4$ and an intracavity photon number $\approx 2 \times 10^{-3}$. The solid line shows a theoretical comparison. The quantitative agreement is reasonable, and we have not included any unaccounted overall scaling factors on the theory. As the intensity increases, a Gaussian background appears. Spontaneous emission events may be the source of the background [26]. Note that the transit time across the cavity waist is 72 ns.

We have performed functional fits of Eq. (17) and an additional Gaussian. A reasonable fit can be made, but the value of $\mathcal{A}$ does not follow from the independently measured values of g and κ. We believe our procedure takes into ac-

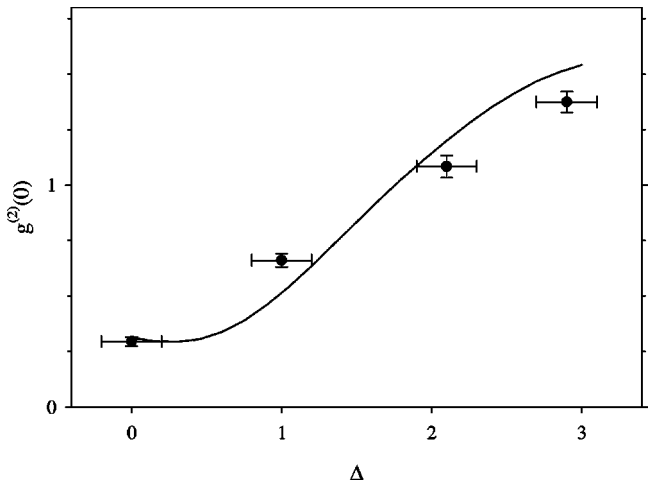

FIG. 7. $g^2(0,\Delta)$ data taken with cavity 4 and $X=0.12$. The nonclassical statistics completely disappear with a detuning of only $\Delta=2$. The line is the theoretical curve described in the text.

count the main mechanisms which reduce the size of nonclassical effects.

C. Detuning

Detunings of either the cavity Θ or the laser from the atomic transition frequency Δ affect the measured nonclassical correlations. The cavity detuning is less of a problem since we actively stabilize the cavity length to stay on resonance, typically to within $\frac{1}{5}\kappa$. A more serious problem is the atomic detuning which is brought about by the cavity mode and the atomic beam not being exactly perpendicular. As mentioned above, we compensate for this shift by adjusting the laser frequency to minimize the cavity tranmission with atoms. The shift in the laser frequency has been as much as 7.5 MHz. Since the beam has a velocity spread in the longitudinal direction, the laser frequency shift does not correct for this, and most interacting atoms have detunings. This decreases the size of the nonclassical effects. We can take this into account using a weighting procedure as discussed above.

Figure 7 demonstrates how the nonclassical feature of sub-Poissonian statistics disappears and the signal becomes noisier with increasing atomic detuning. The plot shows $g^2(0,\Delta)$ and a comparison with theory. The theory is calculated as outlined above. From the known frequency shift of the laser which minimizes the transmission and $g^2(0)$ (7.5 MHz) and the mean atomic velocity (340 m/s), we determine the angle from perpendicular between the beam and mode to be 17.3 mrad. A Gaussian offset of 0.3 is added on resonance $(\Delta=0)$. This offset is scaled by $1/(1+\Delta^2)$ off resonance, as would be expected for spontaneous emission. The theory is in good quantitative agreement with the data. Note that these detuning data were taken at higher intensities than the data of Fig. 6.

On the flip side, we can approach detuning as another knob to probe our system. This leads us to a better understanding of the processes occurring between the atoms and the cavity. We can consider the signal from the cavity to consist of the sum of the coherent driving field and an out-of-phase polarization field from the atoms. This polarization field is squeezed, and the self-homodyning of this squeezed field with the coherent driving field gives rise to the sub-Poissonian statistics that we observe. When we introduce a detuning, the cavity field acquires a phase shift. At $\Delta=1$, the phase is shifted by 45°. The detuning allows us to shift the phase of the field fluctuations that we are sampling. The in-phase and in-quadrature fluctuations exhibit an opposite-phase oscillatory response [26].

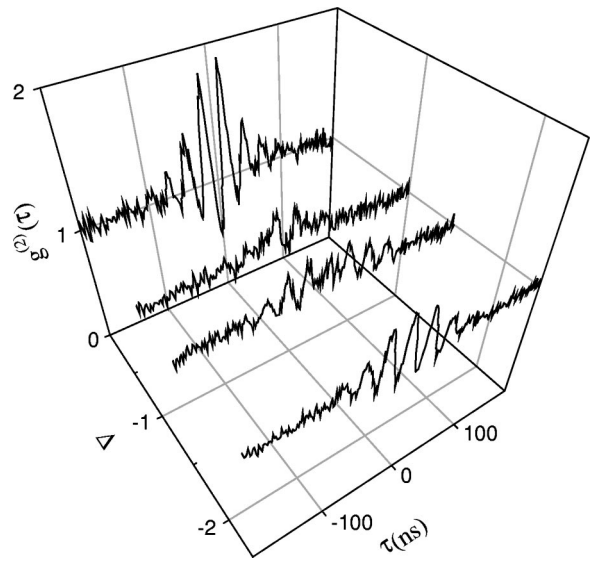

FIG. 8. $g^2(\tau)$ as a function of detuning Δ. These are data taken with cavity 1 with $N\approx 20$ and $X=0.11$.

Figure 8 shows the evolution of the correlations as the laser is detuned from the atomic transition. The effect of detuning is symmetric in Δ. We plot a set of negative detunings for cavity 1 operated with $N=20$. On resonance $(\Delta=0)$, we sample the in-phase component and observe sub-Poissonian antibunching. At $\Delta=-1$, which shifts the phase of the cavity field by 45°, we sample roughly equal portions of the two quadratures. The correlation exhibits a noisy signal with remnants of the large delayed peaks. As we increase to $\Delta=-2.3$, which corresponds to a phase shift of 66°, we sample more of the out-of-phase quadrature, and we observe a classical bunched oscillation which is out of phase with the on-resonance measurement. Note the signal is reduced because as we detune, we also decouple the atoms from the cavity mode. This is qualitatively different from resonance fluorescence where detunings modify the generalized Rabi frequency and lead to oscillations, but do not alter the anti-bunched nature of the observed correlations [21]. We have recently directly measured the cavity field with a conditional homodyne scheme [34], and obtained additional evidence supporting this interpretation.

We can compare the evolution of the frequencies to theory. Figure 9 shows the fast Fourier transforms of the measurements with a comparison from the linearized theory [22]. The agreement is quantitative and very good. The spectrum dies away around $\Delta=1$ and then grows. This is the point where the phase is reversing. These frequencies are

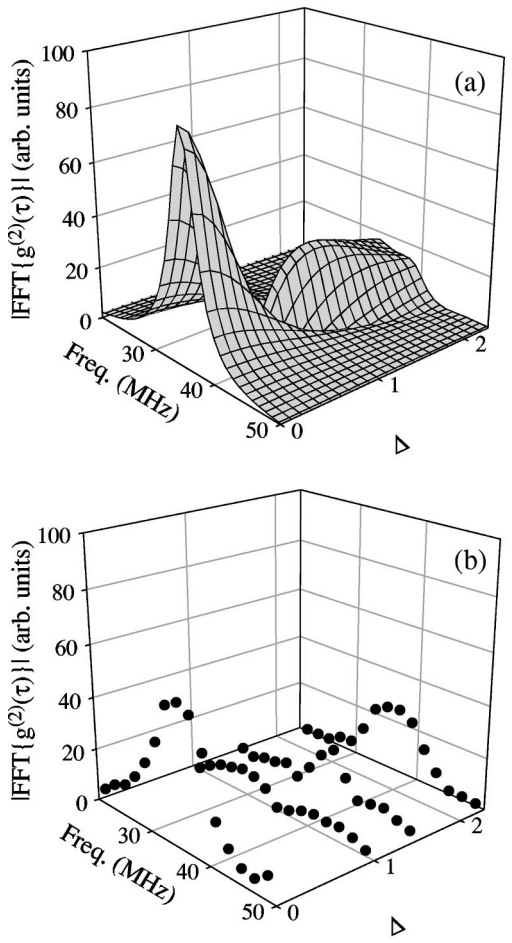

FIG. 9. Magnitude of the fast Fourier transform (FFT) of the $g^{(2)}(\tau)$ as a function of detuning Δ for similar conditions as in Fig. 8: theory (a) and data (b).

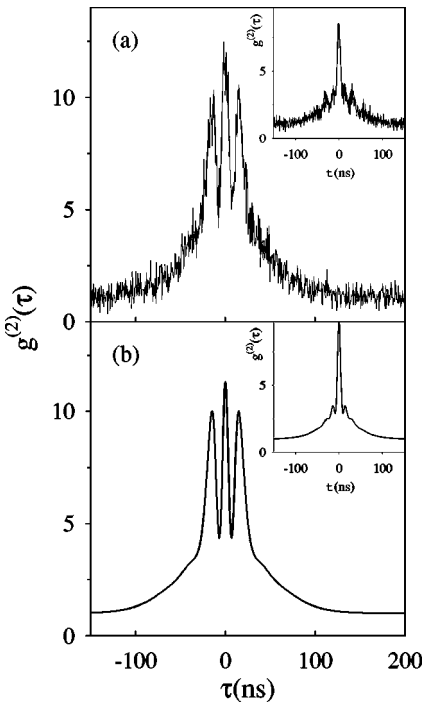

FIG. 10. $g^2(\tau)$ for cavity 3 with a small effective atom number $N\approx 3$, and $X=0.06$. The main plot (a) shows data collected on resonance. The inset shows data with a detuning of $\Delta=1.5$. Plot (b) shows the theoretical calculation for on resonance and off resonance in the inset.

very different than those observed by Brune *et al.* [8] in their work in cavity QED with Rydberg atoms. They exited higher levels of the Jaynes-Cummings ladder, and studied their evolution.

We have observed that the detuning offset needed to bring the laser into resonance with the atoms in the beam can change between data collections. We have traced this to the liquid-nitrogen-cooled surface that is needed to reduce atomic background. The cavity holder also cools during this time, as is evident by a contraction of the cavity length which leads to a drift in the cavity resonance. After a run is over, the system warms back up to room temperature. This cooling and heating causes the different parts of the cavity to contract and expand.

D. Strong coupling

Carmichael *et al.* [24] showed that for large atom-cavity couplings the correlation function exhibits bunching yet still violates classical bounds through the existence of delayed zeros. The mechanism for these zeros is the large jump in the atomic polarization after the escape of a photon from the system, that reverses the sign of the cavity field. As discussed above, the predictions are significantly modified by a variety of effects related to the atomic beam. Nevertheless using cavity 3 (see Table I), which had the strongest coupling of those used ($C_1=9.7, n_0=0.04$), we have observed large bunched oscillations. Figure 10(a) shows the measured correlation function on resonance $\Delta=0$, and for a detuning of $\Delta=1.5$ in the inset. The large size of the oscillations distinguish this from earlier measurements. The features do not violate the Schwarz inequalites [Eqs. (11) and (12)] and the correlation exhibits large bunching. There also appears to be a Gaussian background with $\sigma\approx 50$ ns. The effective number of atoms is low $N\approx 3$, so that fluctuations of the atom number lead to large changes of the coupling and cavity transmission, which contributes to the Gaussian background. However, on top of this, there is still a strong coherent coupling rising above the atomic fluctuations. In Fig. 10(b), we plot the theoretical result using the procedure outlined above. A Gaussian background is added to the final result, but the size and frequency of the oscillations match very well. The size of the Gaussian background decreases as we detune off resonance. The reduction is close to that expected for the reduction of spontaneous emission, $1/(1+\Delta^2)\approx 0.3$. The transit time of the atoms to cross the cavity mode waist is ≈ 100 ns.

E. Number of atoms

The measurements of Rempe *et al.* [10] demonstrated that antibunching persisted with little change in the size between $N=18$ and 110, since $\mathcal{A}$ is independent of N for large numbers of atoms [Eq. (20)]. We have probed over a range of

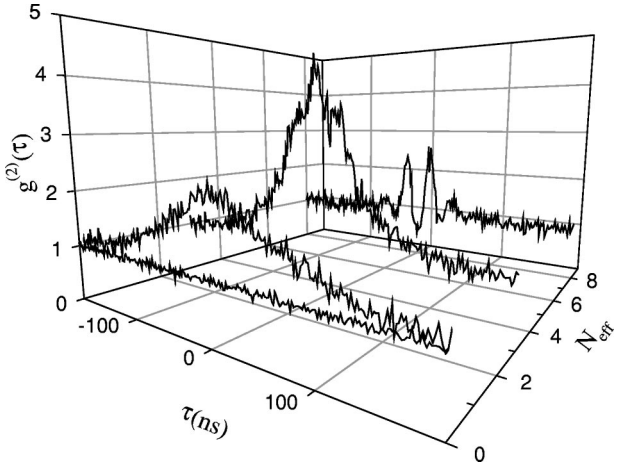

FIG. 11. Evolution of $g^{(2)}(\tau)$ as a function of the effective numner of atoms for $N_{\mathrm{eff}}=0$, 0.1, 3, and 8. Each correlation is taken on resonance. For the cases with atoms, the intracavity intensities were $X=0.2$, 0.06, and 0.03, respectively.

small N, where the qualitative features of the correlation change. Figure 11 shows the evolution of $g^{(2)}(\tau)$ from a small bunched peak to a large bunched peak with hints of oscillations, and then into antibunched oscillations.

For $N=0$, the correlation function is flat, demonstrating the Poissonian statistics of the excitation laser. At a low mean atom number, the peak appears Gaussian with no structure. Recent work with cool atoms launched through a cavity used an intensity correlation measurement to observe light forces on the slowly moving atoms. This was manifested in structure on top of a bunched correlation [35]. Oscillations begin to appear as N increases, on top of a large background similar to that observed in Fig. 10. As the number of effective atoms approaches 10, clear nonclassical features appear: sub-Poissonian statistics and antibunching. The damped oscillatory dynamics of the cavity QED system are also evident in the correlation function.

VII. CONCLUSIONS

We have measured the second-order intensity correlation function of the light emitted from a cavity QED system composed of N two-level atoms coupled to a single mode of the electromagnetic field. The intensity correlations show that the emitted field is nonclassical. The observed features point to an underlying interference phenomenon occurring between the atomic polarization field and the coherent driving field. The dynamical processes are driven by escape of single photons from the cavity system. This escape projects the system in a state out of equilibrium, and we observe the dynamics of the system going to a steady state.

The intensity correlations reveal information about the underlying nonclassical field state produced by the system. The variance of the photon number of the field from the cavity QED system is reduced by a factor of 5 compared to that expected from Poissonian statistics. The nonclassical features are fragile, and degrade significantly with increasing intensity or the presence of atomic detuning. We have obtained quantitative agreement by taking into account experimental factors previously neglected.

We observed how the correlations changed qualitatively as the mean number of atoms interacting changed. Understanding the characteristics of the light emitted from the cavity QED system is necessary if this system is to be used as a source of nonclassical light for other experiments.

ACKNOWLEDGMENTS

We would like to thank Professor Howard J. Carmichael, Professor Perry Rice, and Professor Robert J. Brecha for their interest in this project, and Dr. Christopher Wood for helpful experimental suggestions. In addition, we would like to acknowledge the assistance of Joseph Reiner and Wade Smith with some of the experiments. This work was supported by NSF and ONR.

[1] E. T. Jaynes and F. W. Cummings, Proc. IEEE **51**, 89 (1963).
[2] L. A. Lugiato, in *Progress in Optics*, edited by E. Wolf (North-Holland, Amsterdam, 1984), Vol. XXI, pp. 69–216.
[3] *Cavity Quantum Electrodynamics*, edited by P. R. Berman, Advances in Atomic Molecular, and Optical Physics Supplement 2 (Academic Press, San Diego, 1994).
[4] R. J. Thompson, G. Rempe, and H. J. Kimble, Phys. Rev. Lett. **68**, 1132 (1992).
[5] Y. Zhu, D. J. Gauthier, S. E. Morin, Q. Wu, H. J. Carmichael, and T. W. Mossberg, Phys. Rev. Lett. **64**, 2499 (1990).
[6] G. Rempe, F. Schmidt-Kaler, and H. Walther, Phys. Rev. Lett. **64**, 2783 (1990).
[7] K. An, J. J. Childs, R. R. Dasari, and M. S. Feld, Phys. Rev. Lett. **73**, 3375 (1994).
[8] M. Brune, F. Schmidt-Kaler, A. Maali, J. Dreyer, E. Hagley, J. M. Raimond, and S. Haroche, Phys. Rev. Lett. **76**, 1800 (1996).
[9] D. M. Meekhof, C. Monroe, B. E. King, W. M. Itano, and D. J. Wineland, Phys. Rev. Lett. **76**, 1796 (1996).
[10] G. Rempe, R. J. Thompson, R. J. Brecha, W. D. Lee, and H. J. Kimble, Phys. Rev. Lett. **67**, 1727 (1991).
[11] S. L. Mielke, G. T. Foster, and L. A. Orozco, Phys. Rev. Lett. **80**, 3948 (1998).
[12] J. Gripp, S. L. Mielke, L. A. Orozco, and H. J. Carmichael, Phys. Rev. A **54**, R3746 (1996).
[13] J. Gripp, S. L. Mielke, and L. A. Orozco, Phys. Rev. A **56**, 3262 (1997).
[14] R. J. Brecha, L. A. Orozco, M. G. Raizen, M. Xiao, and H. J. Kimble, J. Opt. Soc. Am. B **12**, 1219 (1995).
[15] S. L. Mielke, G. T. Foster, J. Gripp, and L. A. Orozco, Opt. Lett. **22**, 325 (1997).
[16] H. J. Carmichael, *An Open Systems Approach to Quantum Optics* (Springer-Verlag, Berlin, 1993).
[17] P. D. Drummond, IEEE J. Quantum Electron. **QE17**, 301 (1981).

[18] G. Rempe, R. J. Thompson, R. J. Brecha, Q. Turchette, and H. J. Kimble, in *Atomic Physics 13*, edited by H. Walther, T. W. Hänsch, and B. Neizert, AIP Conf. Proc. No. 275 (AIP, New York, 1993), p. 305.
[19] P. R. Rice and H. J. Carmichael, IEEE J. Quantum Electron. **QE24**, 1351 (1988).
[20] H. J. Kimble, M. Dagenais, and L. Mandel, Phys. Rev. Lett. **39**, 691 (1977).
[21] L. Mandel and E. Wolf, *Optical Coherence and Quantum Optics* (Cambridge University Press, New York, 1995).
[22] R. J. Brecha, P. R. Rice, and M. Xiao, Phys. Rev. A **59**, 2392 (1999).
[23] H. J. Carmichael, S. Singh, R. Vyas, and P. R. Rice, Phys. Rev. A **39**, 1200 (1989).
[24] H. J. Carmichael, R. J. Brecha, and P. R. Rice, Opt. Commun. **82**, 73 (1991).
[25] H. J. Carmichael, Phys. Rev. A **33**, 3262 (1986).
[26] H. J. Carmichael (private communication).
[27] J. P. Clemens and P. R. Rice (unpublished).
[28] A. T. Rosenberger, L. A. Orozco, P. D. Drummond, and H. J. Kimble, Phys. Rev. A **43**, 6284 (1991).
[29] H. J. Carmichael and B. C. Sanders, Phys. Rev. A **60**, 2497 (1999).
[30] R. W. P. Drever, J. L. Hall, F. V. Kowalski, J. Hough, G. M. Ford, A. J. Munley, and H. Ward, Appl. Phys. B: Photophys. Laser Chem. **31**, 97 (1983); J. L. Hall, L. Hollberg, T. Baer, and H. G. Robinson, Appl. Phys. Lett. **39**, 680 (1981).
[31] A. L. Lacaita, F. Zappa, S. Bigliardi, and M. Manfredi, IEEE Trans. Electron Devices **ED40**, 577 (1993).
[32] G. T. Foster, S. L. Mielke, and L. A. Orozco, J. Opt. Soc. Am. B **15**, 2646 (1998).
[33] S. L. Mielke, Ph.D. thesis, State University of New York at Stony Brook, 1998.
[34] G. T. Foster, L. A. Orozco, H. M. Castro-Beltran, and H. J. Carmichael (unpublished).
[35] P. Munstermann, T. Fischer, P. Maunz, P. W. H. Pinkse, and G. Rempe, Phys. Rev. Lett. **82**, 3791 (1999).